NASA TECHNICAL NOTE

NASA TN D-4657

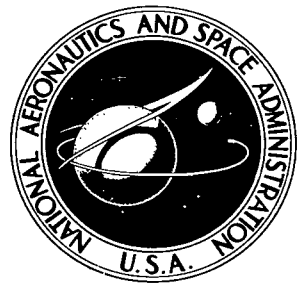

NASA TN D-4657

USE OF PLANETARY OBLATENESS FOR PARKING-ORBIT ALINEMENT

by Joseph R. Thibodeau III

Manned Spacecraft Center
Houston, Texas

NATIONAL AERONAUTICS AND SPACE ADMINISTRATION • WASHINGTON, D. C. • JULY 1968

USE OF PLANETARY OBLATENESS FOR PARKING-ORBIT ALINEMENT

By Joseph R. Thibodeau III

Manned Spacecraft Center
Houston, Texas

NATIONAL AERONAUTICS AND SPACE ADMINISTRATION

For sale by the Clearinghouse for Federal Scientific and Technical Information
Springfield, Virginia 22151 – CFSTI price $3.00

ABSTRACT

A rapid analytical technique is used to determine simultaneously the possible configurations of an elliptical parking orbit at Mars. Both the geometry of planetary approach and departure and the effects of planetary oblateness are used to determine the characteristics of those orbits which shift into proper alinement for departure and require no discrete propulsive maneuvers. The technique makes use of the separable nature of the equations that express secular rotation of the orbit plane and major axis. Preliminary results indicate that the orbital inclinations fall into narrow bands which are widely distributed over the interval of possible inclinations.

USE OF PLANETARY OBLATENESS FOR PARKING-ORBIT ALINEMENT

By Joseph R. Thibodeau III
Manned Spacecraft Center

SUMMARY

A technique relying upon the effects of gravitational harmonics for parking-orbit alinement is analyzed. The basic approach is to choose orbital eccentricity and inclination so that the resulting nodal and apsidal motions will shift the original orbit into proper alinement for departure on the intended date. Thus, the need for propulsive maneuvers to change the orbital inclination, line of apsides, or orbital eccentricity are reduced or eliminated; and periapsis impulses can be used for both the capture and the escape maneuvers. Numerical results are presented for a long-stay-time Mars mission in 1977. These results illustrate the proposed technique, but do not include comparisons with alternative methods.

INTRODUCTION

During planetary capture and landing missions, long-duration parking orbits may be established about the target planet. These stopover missions often require substantial, and sometimes costly, readjustment of the parking orbit to provide for efficient planetary escape and return to Earth. Rotation of the parking orbit becomes necessary to compensate for two dynamic effects: (1) the orientation and motion of the hyperbolic departure asymptote and (2) the motion of the parking orbit resulting from the asphericity of the planetary gravitational field.

Efficient propulsive techniques are available to accommodate the two dynamic effects (ref. 1). These techniques require auxiliary maneuvers, which may be either discrete or combined with the planetary capture and escape maneuvers, to accomplish orbital readjustment.

Nominal missions which require no auxiliary maneuvers can be designed by relying on the effects of the gravitational harmonics. This technique was originally proposed in references 2 and 3. An analytical approach to the technique will be discussed. This technique accommodates both the geometry of approach and departure and the effects of planetary oblateness. It also permits a variety of elliptical parking orbits to be simultaneously found.

The technique is intended for application in preliminary trajectory design and early feasibility studies of orbital missions. In these instances, analytical techniques can be used advantageously to evaluate many possible configurations of the parking orbit. The method is particularly useful for the study of eccentric parking orbits which match so-called "double-Hohmann" transfers, or minimum-energy members of the conjunction class of Mars missions. Conjunction-class missions generally have total trip times of 950 to 1000 days with stay times ranging from 300 to 500 days. For these missions, there is sufficient time for perturbations to rotate high-eccentricity parking orbits through large angles. This method is somewhat less successful for the study of parking-orbit configurations required for the opposition-class missions in which stay times on the order of 40 days are investigated. For these short stay times, fewer parking-orbit configurations are available, and the parking orbits generally have low eccentricities.

Only secular rotation of the orbital plane and major axis due to planetary oblateness is considered. Orbital realinement is produced by rotation of the orbit line of nodes and the line of apsides, and these rotations are primarily the result of planetary oblateness. In the presence of a third body, there are long-period rotation rates caused by coupling of the oblateness and third-body perturbations (described in refs. 4 and 5). In addition, resonances can lead to feedback between the orbit and the perturbing function (ref. 6).

In general, inclusion of a third body and the higher order harmonics of the planetary gravitational field requires numerical integration. The technique developed in this report can be used as a tool for preliminary mission planning. This technique permits rapid determination of all possible parking-orbit configurations. Orbits which best meet the required ground rules or boundary conditions can then be selected for further study using precision techniques.

The author wishes to thank Victor R. Bond for the use of the interplanetary trajectory-analysis program for the example mission.

SYMBOLS

a	semimajor axis
C	auxiliary variable defined by equation (20)
c_1, c_2, c_3, c_4	constant coefficients of a fourth-order polynomial
e	orbital eccentricity
i	orbital inclination with respect to the planetary equatorial plane
J_2	second zonal harmonic

$$K = (1 - e)^{3/2}(1 + e)^{-2} = \frac{\dot{\Omega}_r}{C}$$

n	mean motion of the parking orbit
R	planetary equatorial radius
r_p	radius of periapsis
T_o	parking-orbit regression time
T_s	stay time in parking orbit
t_Ω	rotation time of orbital node
t_ω	rotation time of periapsis vector
V_∞	hyperbolic excess velocity
$\hat{V}_\infty$	unit vector of hyperbolic excess velocity
X, Y, Z	coordinates in the planetocentric system
α	planetocentric longitude
ΔV	impulsive velocity
δ	planetocentric declination
θ	auxiliary angle defined by equation (4)
μ	gravitational parameter
σ	auxiliary variable = $\sin^{-1}(\tan \delta / \tan i)$
Ω	ascending node
$\hat{\Omega}$	unit vector in the direction of the ascending node
$\dot{\Omega}_r$	normalized rotation rate
$\dot{\Omega}_s$	nodal regression rate
ω_p	argument of periapsis
$\dot{\omega}_s$	periapsis precession rate

Subscripts:

A	approach trajectory
D	departure trajectory
h	hyperbola
p	periapsis
Ω_1	ascending node closer to the V_∞ vector, defined by equation (1) and figure 2
Ω_2	ascending node farther from the V_∞ vector, defined by equation (1) and figure 2

ANALYSIS

Technique for Orbital Alinement

The sequence of maneuvers for the orbital-alinement technique is illustrated in figure 1 and is outlined as follows:

1. Orbital insertion occurs at periapsis of the arrival hyperbola. At the time of periapsis passage, the following conditions exist:

   a. The parking orbit and the arrival hyperbola are coplanar.

   b. The periapsis position vectors of the parking orbit and arrival hyperbola are identical.

2. During the orbital coast phase, orbital perturbations continually rotate the orbital plane and major axis, thereby shifting the parking orbit into alinement with the nominal departure asymptote.

3. At the nominal time of departure, orbital launch occurs at periapsis of the parking orbit, and the following conditions exist:

   a. The parking orbit and the departure hyperbola are coplanar.

   b. The periapsis position vectors of the parking orbit and departure hyperbola are identical.

The technique implicitly defines two constraints or boundary conditions; continuity of the periapsis position and of the orbital inclination must be enforced at the match points of the parking orbit and the arrival and departure hyperbolas. For this

analysis, radius of periapsis and orbital inclination can be regarded not only as continuous but constant, since planetary oblateness does not contribute secular rates of change to either parameter.

The boundary conditions for the maneuver sequence are defined by four quantities which are the necessary problem input data:

1. Radius of periapsis r_p

2. Orbital stay time T_s

3. Hyperbolic excess velocity of the approach trajectory $V_{\infty, A}$

4. Hyperbolic excess velocity of the departure trajectory $V_{\infty, D}$

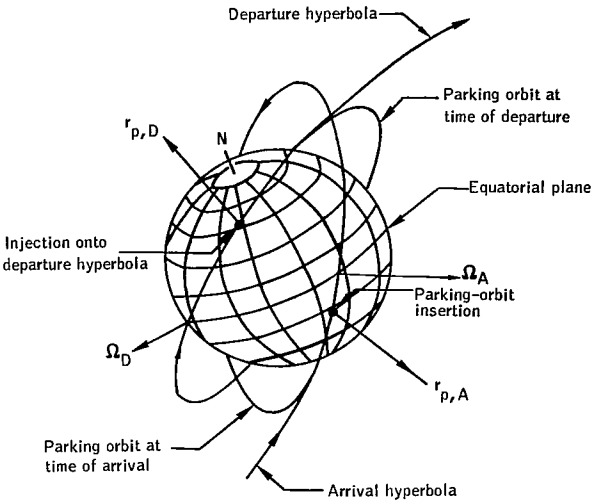

Figure 1. - Geometry of the parking orbit at the time of arrival and departure.

These data are calculated by an independent trajectory-analysis program. The interplanetary trajectory is therefore assumed to be known, and only those operations inside the planetary sphere of influence are considered.

Derivation

The following parameters are used to define the parking orbit:

1. Inclination i

2. Eccentricity e

3. Radius of periapsis r_p

4. Longitude of the ascending node α_Ω

5. Argument of periapsis ω_p

The analysis shows how these parameters are found for regressing parking orbits which shift into proper alinement for departure. The orbital parameters are referenced to the time of periapsis passage on the arrival hyperbola.

The approach relies on the separable nature of the equations which express secular rotations of the orbit plane and major axis. These secular rotation rates are functions of inclination and eccentricity. The technique allows the inclination function to be

separated from the eccentricity function, thereby permitting calculation of the required orbit inclination independently of eccentricity.

The determination of the orbital parameters thus involves two distinct phases. The first phase is a search for the orbital inclination, ascending node, and periapsis vector. The orbital inclination is found by choosing it as the independent search variable. By sweeping through the range of possible inclinations, a parametric search table is generated, and the proper orbital parameters are then found by interpolation. The second phase is a search for the orbital eccentricity. The eccentricity is found by using the Newton-Raphson method.

Planetocentric coordinate system. - It is assumed that the hyperbolic excess velocities are referenced to an inertial planetocentric coordinate system. Since interplanetary trajectories are generally calculated in a heliocentric reference, these velocities must be transformed into this coordinate system. The positive Z-axis of the planetocentric coordinate system points north along the planetary axis of rotation. The XY-plane is defined by the planetary equatorial plane. The positive X-axis is defined by the intersection of the planetary orbit and equatorial planes and corresponds to the descending node of the planetary orbit on the equatorial plane. The positive Y-axis is 90° east of X and completes a right-handed system.

Further discussion of this coordinate system and a presentation of Mars transformation equations are provided in reference 7. The position of the North Pole and the physical ephemeris of Mars are also discussed in reference 8.

Basic equations. - Assuming that the respective hyperbolic excess velocities and the radius of periapsis are specified, the following equations define the planetocentric longitude of the ascending node and the argument of periapsis of both the planetary capture and the planetary escape hyperbolas. These data will be used later to determine the inclination of the parking orbit.

The node and periapsis position vectors are double-valued functions of inclination. This can be seen in figure 2, which shows that two orbital planes contain the V_∞ vectors for all inclinations.

The longitude of the ascending node α_Ω is determined from

$$\left.\begin{aligned} \alpha_{\Omega_1} &= \alpha - \sigma \\ \alpha_{\Omega_2} &= \alpha + \sigma + \pi \end{aligned}\right\} \qquad (1)$$

where $\sigma = \sin^{-1}(\tan \delta / \tan i)$, and α and δ are the planetocentric longitude and

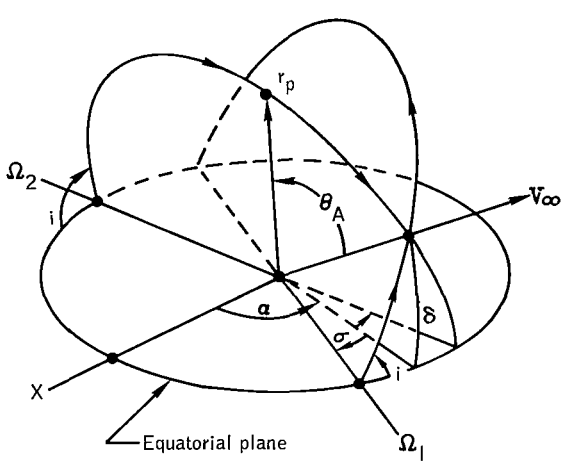

Figure 2. - Geometry of trajectory planes.

declination of the V_∞ vector. As shown in figure 2, α_{Ω_1} is the longitude of the ascending node closer to the V_∞ vector. Likewise, α_{Ω_2} is the longitude of the node farther from the V_∞ vector. The declination of the V_∞ vector defines the minimum orbital inclination, since σ is not defined for i less than δ.

The semimajor axis of the approach hyperbola a_h is determined from the vis viva equation

$$a_h = \frac{\mu}{V_{\infty,A}^2} \tag{2}$$

When the radius of periapsis is specified, the eccentricity of the approach hyperbola is

$$e_h = \frac{r_p}{a_h} + 1 \tag{3}$$

The angle between the arrival V_∞ vector and the periapsis of the approach hyperbola can now be found by

$$\theta = \cos^{-1}\left(\frac{1}{e_h}\right) \tag{4}$$

where e_h is the eccentricity of the approach hyperbola.

The argument of periapsis ω_p for the approach hyperbola is

$$\omega_p = \cos^{-1}\left(\hat{\Omega} \cdot \hat{V}_\infty\right) - \theta \tag{5}$$

At the time of periapsis passage, the argument of periapsis of the parking orbit is the same as that for the approach hyperbola.

Equations (1) to (5) are used to find the node and periapsis vectors at the time of injection onto the departure hyperbola, with the following exception:

$$\theta = \cos^{-1}\left(\frac{-1}{e_{h,D}}\right) \tag{6}$$

where $e_{h,D}$ is the eccentricity of the departure hyperbola.

Determination of orbital inclination. - The longitude of the ascending node α_Ω and the argument of periapsis ω_p are now assumed to have been calculated for the node closest to the V_∞ vector for both the arrival and the departure hyperbolas, and the parking orbit shown in figure 1 is considered once again. During the planetary stay time, the ascending node of the approach hyperbola must move to the ascending node of the departure hyperbola, and $r_{p,A}$ must move to $r_{p,D}$.

The angular distance the parking-orbit node must travel is

$$\Delta\alpha_\Omega = \alpha_{\Omega,D} - \alpha_{\Omega,A} = f\left(V_{\infty,A}, V_{\infty,D}, r_p, i\right) \tag{7}$$

where the subscripts A and D indicate the arrival and departure hyperbolas, respectively. Likewise, the angular distance the periapsis vector must travel is

$$\Delta\omega_p = \omega_{p,D} - \omega_{p,A} = g\left(V_{\infty,A}, V_{\infty,D}, r_p, i\right) \tag{8}$$

The speed of rotation of the node $\dot{\Omega}_s$ and periapsis $\dot{\omega}_s$ because of secular variation J_2 is given in reference 9 as

$$\dot{\Omega}_s = \frac{-3nJ_2R^2}{2a^2\left(1 - e^2\right)^2}\cos i \tag{9}$$

$$\dot{\omega}_s = \frac{-3nJ_2R^2}{2a^2\left(1 - e^2\right)^2}\left(\frac{5}{2}\sin^2 i - 2\right) \tag{10}$$

The time for the parking-orbit node to traverse $\Delta\alpha_\Omega$ is

$$t_\Omega = \frac{\Delta\alpha_\Omega}{\dot{\Omega}_s} \tag{11}$$

and the time for the periapsis to traverse $\Delta\omega_p$ is

$$t_\omega = \frac{\Delta\omega_p}{\dot{\omega}_s} \tag{12}$$

If the stay time in the parking orbit is designated by T_s, the problem is to obtain the inclination and eccentricity of the parking orbit such that

$$T_s = t_\Omega = t_\omega \tag{13}$$

This condition is obtained in two steps: (1) A parking-orbit inclination that will make t_Ω equal to t_ω is found, and (2) the parking-orbit eccentricity is adjusted to make t_Ω and t_ω equal to the planetary stay time T_s.

It should be noted that a closed-form solution is not evident. If equations (11) and (12) are equated, a solution for the inclination would then be found in terms of $\Delta\alpha_\Omega$ and $\Delta\omega_p$. But $\Delta\alpha_\Omega$ and $\Delta\omega_p$ are not known, since they are likewise functions of orbital inclination, as is shown by equations (7) and (8).

A simple interpolation scheme lends itself to finding the orbital inclination for which t_Ω equals t_ω. The basic equations are used to calculate t_Ω and t_ω at 10° increments through the interval of possible inclinations. The ratio t_Ω/t_ω can be tabulated with inclination, and the equality of t_Ω and t_ω is indicated by a ratio of 1. Thus the table can be scanned to find all the time ratios near 1, and the possible parking-orbit inclinations can be found by interpolation. If necessary, the previously discussed procedure can be repeated, using a smaller inclination increment to make t_Ω and t_ω equal within some specified tolerance.

In practice, not one, but four ratio-versus-inclination tables are simultaneously generated. As shown in figure 2, there are two trajectory planes containing the approach asymptote for every inclination. Thus, there are two ways by which the

parking orbit can be alined with the approach asymptote. Also, there are two ways for the parking orbit to shift into alinement with the departure asymptote. In conclusion, there are four basic geometries of planetary approach and departure which can be accommodated by a regressing parking orbit. All four geometries must, of course, be scanned to insure finding all available parking orbits.

Determination of orbital eccentricity. - The orbital eccentricity must now be adjusted so that the orbit will rotate the required amount during the planetary stay time T_s. A circular orbit would rotate through the required angles during the time T_o.

A simple test for the existence of an elliptical orbit that regresses the proper amount during the stay time T_s is $T_o < T_s$. Since circular orbits have the fastest regression rates, this inequality means that the eccentricity can be increased to slow down the speed of rotation and thereby force T_o to equal T_s.

The eccentricity that makes T_o equal to T_s can be found quite readily by the Newton-Raphson technique. The orbital eccentricity is a real root of a fourth-order polynomial found by expressing equation (9) or (10) in terms of the eccentricity. The derivation of this polynomial and the solution for orbital eccentricity follow.

The rate of secular variation of the node and periapsis vectors has been given by

$$\dot{\Omega}_s = \frac{-3nJ_2R^2}{2a^2\left(1 - e^2\right)^2} \cos i \tag{9}$$

$$\dot{\omega}_s = \frac{-3nJ_2R^2}{2a^2\left(1 - e^2\right)^2} \left(\frac{5}{2} \sin^2 i - 2\right) \tag{10}$$

The rate ratio $\dot{\Omega}_s/\dot{\omega}_s$ is determined by the inclination since the terms involving eccentricity divide out in the ratio. Thus, the eccentricity can be adjusted independently to change the rate without destroying a particular value of the ratio.

Designating the common factor in both equations by $\dot{\Omega}_r$, then

$$\dot{\Omega}_r = \frac{-3nJ_2R^2}{2a^2\left(1 - e^2\right)^2} \tag{14}$$

and equations (9) and (10) become

$$\dot{\Omega}_s = \dot{\Omega}_r \cos i \tag{15}$$

$$\dot{\omega}_s = \dot{\Omega}_r\left(\frac{5}{2}\sin^2 i - 2\right) \tag{16}$$

The mean motion n is

$$n = \sqrt{\frac{\mu}{a^3}} \tag{17}$$

and the semimajor axis a is

$$a = \frac{r_p}{1 - e} \tag{18}$$

By substituting equations (17) and (18) for n and a into equation (14) and simplifying, the following result is obtained:

$$\dot{\Omega}_r = \left(-\frac{3}{2}\sqrt{\mu}J_2R^2r_p^{-7/2}\right)(1 - e)^{3/2}(1 + e)^{-2} \tag{19}$$

For a given radius of periapsis, the quantity $-\frac{3}{2}\sqrt{\mu}J_2R^2r_p^{-7/2}$ is constant. If

$$C = -\frac{3}{2}\sqrt{\mu}J_2R^2r_p^{-7/2} \tag{20}$$

then

$$K = (1 - e)^{3/2}(1 + e)^{-2} \tag{21}$$

where

$$K = \frac{\dot{\Omega}_r}{C} \tag{22}$$

Given K, the problem now is to find e. Squaring both sides of equation (21) and simplifying, the result is

$$K^2(1 + e)^4 = (1 - e)^3 \tag{23}$$

Expanding equation (23) in a binomial expansion and collecting common powers of e results in

$$e^4 + \frac{\left(4K^2 + 1\right)}{K^2} e^3 + \frac{\left(6K^2 - 3\right)}{K^2} e^2 + \frac{\left(4K^2 + 3\right)}{K^2} e + \frac{K^2 - 1}{K^2} = 0 \tag{24}$$

Equation (24) will have a real root on the interval $0 \leq e < 1$, provided $T_o \leq T_s$. Also, equation (24) is of the form

$$f(x) = x^4 + c_1x^3 + c_2x^2 + c_3x + c_4 = 0 \tag{25}$$

and the derivative with respect to x of equation (25) is

$$f'(x) = 4x^3 + 3c_1x^2 + 2c_2x + c_3 = 0 \tag{26}$$

The constant coefficients in equations (25) and (26) are

$$\left.\begin{aligned} c_1 &= \frac{4K^2 + 1}{K^2} & c_2 &= \frac{6K^2 - 3}{K^2} \\ c_3 &= \frac{4K^2 + 3}{K^2} & c_4 &= \frac{K^2 - 1}{K^2} \end{aligned}\right\} \tag{27}$$

and the constant K is easily evaluated as

$$K = \frac{\dot{\Omega}_r}{C} = \frac{\dot{\Omega}_s}{C \cos i} = \frac{\Delta\alpha_\Omega / T_s}{C \cos i} \tag{28}$$

where C is the quantity specified in equation (20).

The parking-orbit eccentricity is found by iteration using equations (25) and (26) in

$$e_{n+1} = e_n - \frac{f(e_n)}{f'(e_n)} \tag{29}$$

Since e is between 0 and 1, the iteration using equation (29) quickly converges when an initial estimate of $e = 0.5$ is used.

A parking-orbit analysis program. - The technique discussed has been programed, and the program is essentially a search routine. It accepts two V_∞ vectors, one for the approach trajectory and one for the departure trajectory. The V_∞ vectors define a range of permissable values of inclination for the approach and departure trajectories.

The program scans all the possible inclinations and then uses the previously discussed interpolation scheme and a Newton-Raphson technique to determine the characteristics of those parking orbits which match the approach and departure trajectories.

In general, more than one feasible orbit exists. The program determines all parking-orbit configurations which match the arrival and departure trajectories. The output consists of the Keplerian elements of the parking orbit, the approach hyperbola, and the departure hyperbola. The orbital parameters of the parking orbit are referenced to the time of periapsis passage on the approach hyperbola.

EXAMPLE — 1977 MARS ORBITAL MISSION

The following example is a preliminary analysis of the parking-orbit phase of a near-minimum-energy Mars-orbital mission beginning in 1977. The example illustrates the characteristics of regressing parking orbits which are typical of long-stay-time Mars-orbital missions. It also shows how the required characteristics of the Mars parking orbit change as the launch date is varied through the Earth-orbital launch window. No comparisons are made with alternative methods for parking-orbit alinement; however, supporting data are included so that evaluations can be made.

The interplanetary trajectories and the hyperbolic excess velocities were calculated by an independent program. The Earth-orbital launch dates, the trip times, and the Mars-orbital stay times were selected so that the heliocentric trajectories would be near-Hohmann transfers. These data are shown in figure 3. The Earth-to-Mars trip time varied between 360 and 320 days. The Mars-orbital stay time (300 days) and the return trip time (320 days) were held constant through the Earth-orbital launch window. The total trip time thus varied between 980 and 940 days. The variation of the V_∞ magnitudes is shown in figure 4.

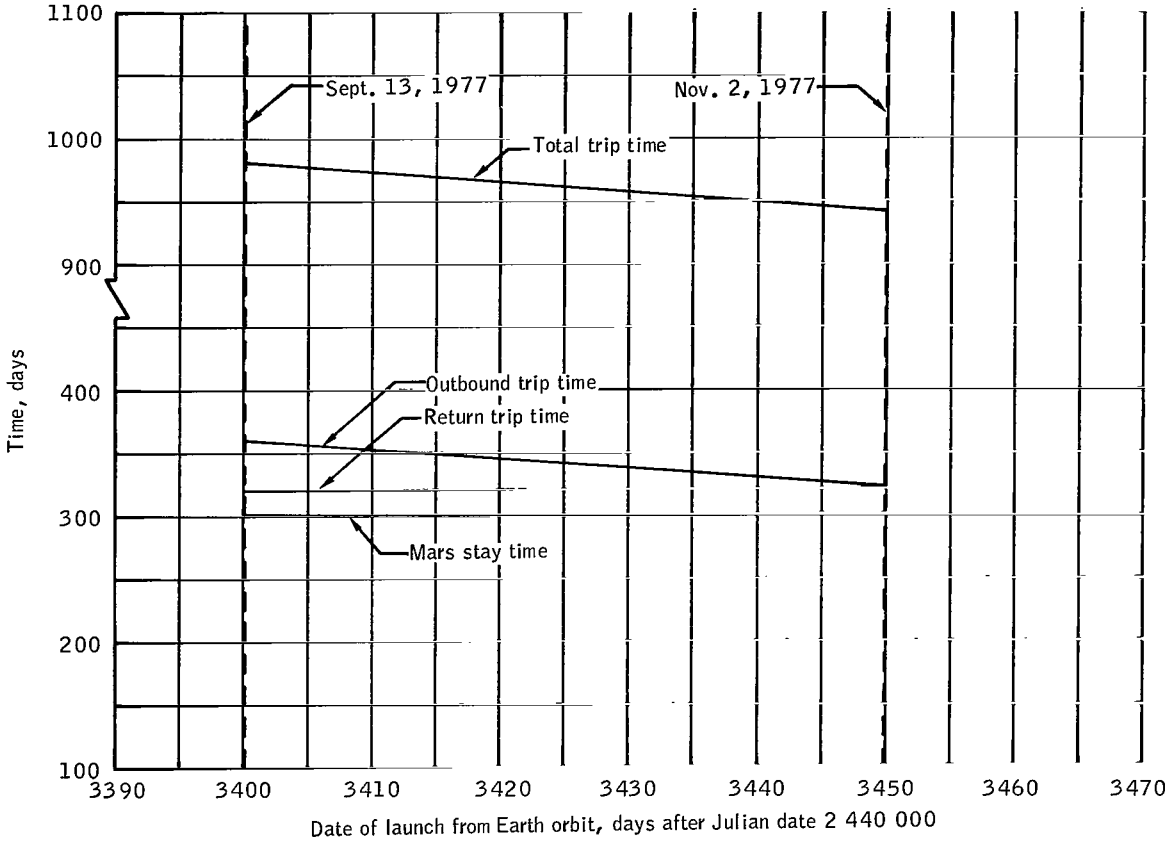

Figure 3. - Variation of trip times during the Earth-orbital launch window for a low-energy Mars-orbital mission beginning in 1977.

The variation of the ΔV requirements is shown in figure 5. Earth-orbital launch begins from a circular parking orbit at an altitude of 262 n. mi. The parking orbit is coplanar with the Earth departure hyperbola. The Mars-orbital insertion (MOI) and transearth injection (TEI) impulsive velocities are, of course, dependent on the type of parking orbit which is used at Mars. The MOI and TEI impulsive velocities are shown for the highest energy regressing parking orbit (orbit 1, table I), which shifts into proper alinement for departure. (The orbital geometry code is presented in table II.) The Earth entry velocity ($\sim$38 000 fps) is indicated for an entry altitude of 400 000 feet.

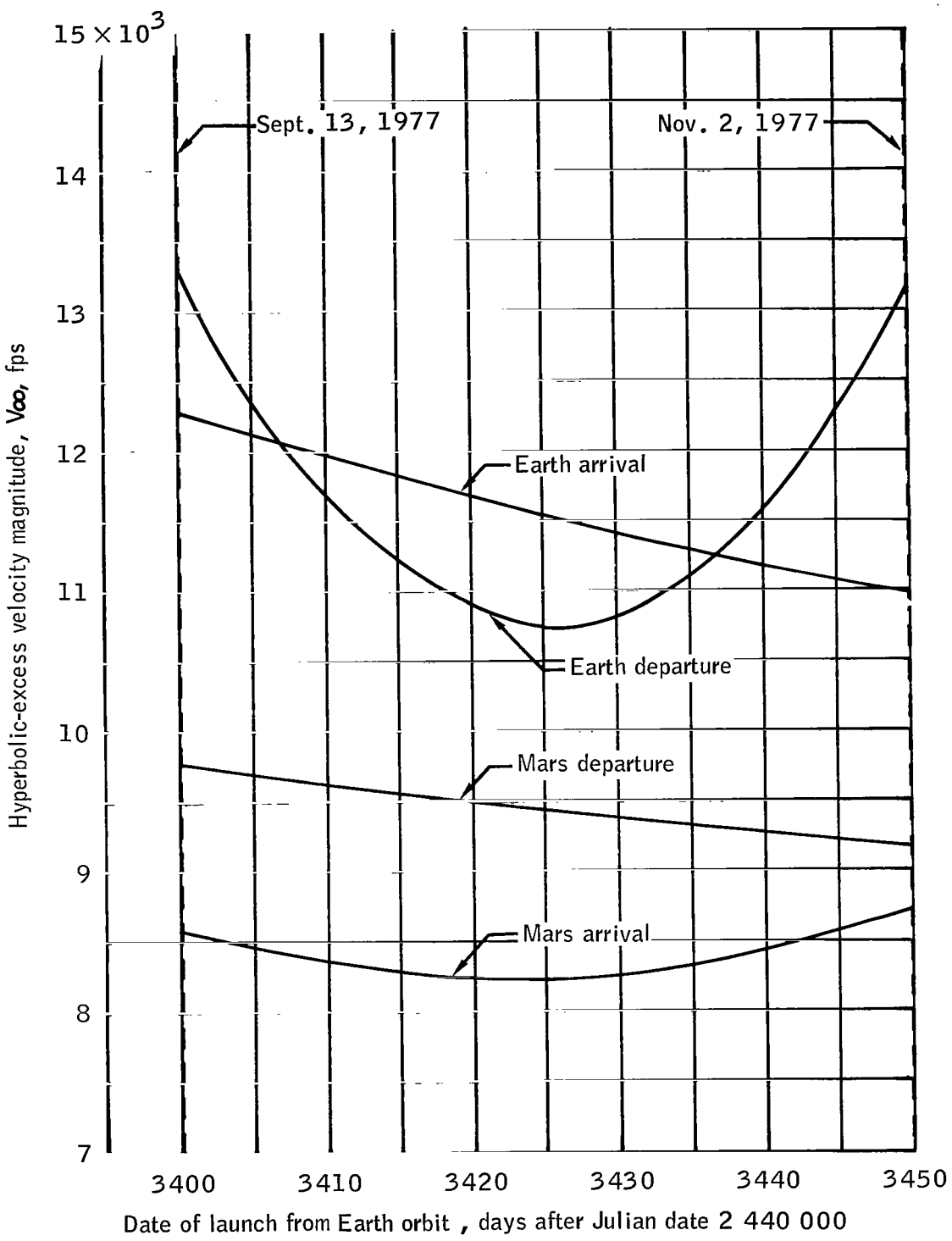

Figure 4. - Variation of the V_∞ magnitudes.

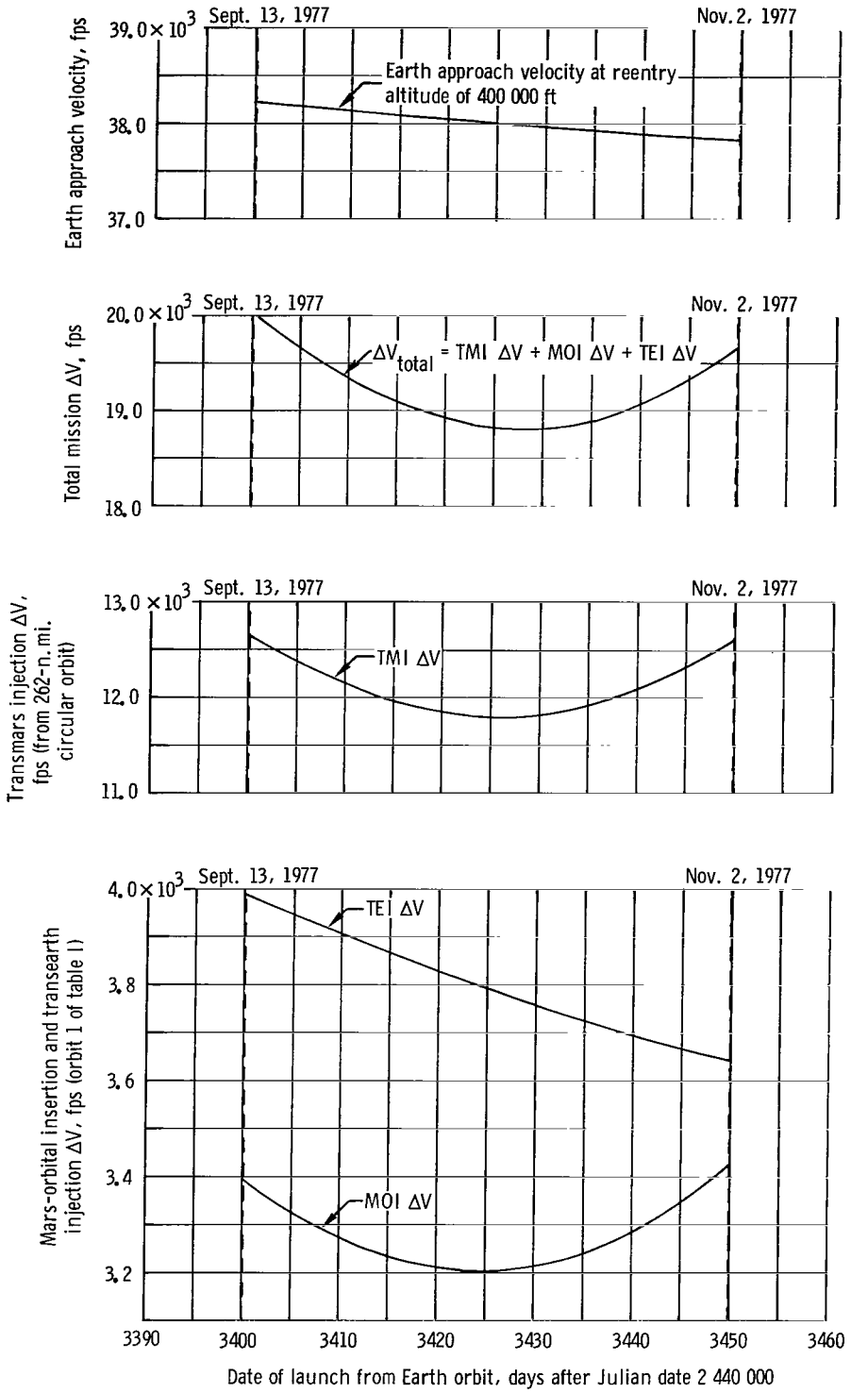

Figure 5. - Variation of ΔV requirements.

RESULTS

Ten parking orbits were found to shift into proper alinement for departure. The characteristics of these orbits are shown in table I. All the orbits have periapsis altitudes of 200 n. mi. It should be noted that these orbits represent a set of the highest energy parking orbits which shift into proper alinement for departure. There are other sets of lower energy orbits which also shift into proper alinement. These sets are found by adding integral multiples of 2π to the required angles of rotation of the orbital node $\Delta\alpha_\Omega$ and argument of periapsis $\Delta\omega_p$. In equations (11) and (12), integral multiples of 2π can be added to either $\Delta\alpha_\Omega$ or $\Delta\omega_p$ or both. The resultant parking orbits can thus be forced to complete a full revolution or multiple revolutions of either the orbital node or the periapsis vector prior to final alinement with the departure asymptote.

Table I summarizes the parking orbits available at the beginning, middle, and end of the 50-day mission window. The parking orbits are classified into four categories corresponding to the four basic geometries of planetary approach and departure. If Ω_1 and Ω_2 are used to designate the two configurations of the parking orbit according to equation (1) and figure 2, then the four geometries can be designated as shown in table II.

These orbits exhibit several interesting properties. The orbital inclinations fall into narrow bands which are widely distributed over the interval of possible inclinations. Also, the orbital eccentricity is correlated with the orbital inclination. In general, parking orbits with low inclinations have higher eccentricities than more highly inclined parking orbits.

The orbital inclinations are determined in essence by the geometry of planetary approach and departure and by the ratio of the required angles of rotation of the orbital node and periapsis vectors $\Delta\alpha_\Omega$ and $\Delta\omega_p$. The orbital inclination is determined so that the ratio of the orbital rotation rates $\dot{\Omega}_s/\dot{\omega}_s$ is equal to the ratio of the required angles of rotation $\Delta\alpha_\Omega/\Delta\omega_p$. The result is that when the required angles of rotation are equal and in opposite directions, the rotation rates must likewise be equal and in opposite directions. This can occur at inclinations of 46.4° and 106.8°. Similarly, when the required angles of rotation are equal and in the same direction, the rotation rates must be equal and in the same direction. This situation can occur at inclinations of 73.2° and 133.6°. It would not be surprising, then, if the inclinations of regressing orbits fall into narrow regions centered on or somewhere near these equal-rate inclinations. This is the case illustrated in figure 6, which shows the bands of inclination of regressing orbits superimposed on a plot of the nodal and periapsis rotation rates. For an arbitrary V_∞ geometry, the inclination bands can be shifted to either side of the equal-rate inclinations. In cases where the orbit is required to shift through integral multiples of 2π prior to final alinement, the bands will occur at different characteristic values of inclination.

It was pointed out that parking orbits with low inclinations have higher eccentricities than more highly inclined parking orbits. This result can be seen intuitively in figure 6. The figure indicates that near-equatorial orbits characteristically have faster rotation rates than near-polar orbits and that their speed of rotation is less dependent on eccentricity. Thus, if two parking orbits with identical nodal and periapsis rotation rates — one a near-polar orbit and the other a near-equatorial orbit — are considered, the near-equatorial orbit will have the larger eccentricity. For example, if two orbits have inclinations of 46.4° and 106.8° (the inclinations for which the rotation rates are equal and opposite), the 46.4°-inclination orbit has higher rotation rates than the 106.8°-inclination orbit. Thus, the eccentricity of the 46.4°-inclination orbit must be increased to slow its rates enough to match those of the 106.8°-inclination orbit.

Further evidence of the behavior is shown in figure 7. Figure 7 shows the variation of the orbital eccentricity with stay time for a hypothetical, non-varying

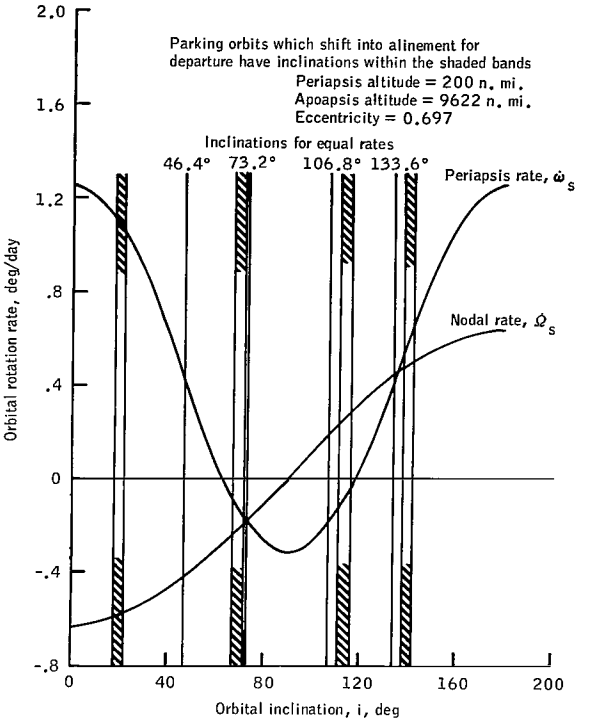

Figure 6. - Secular rotation rates of the parking-orbit node and periapsis vectors due to planetary oblateness.

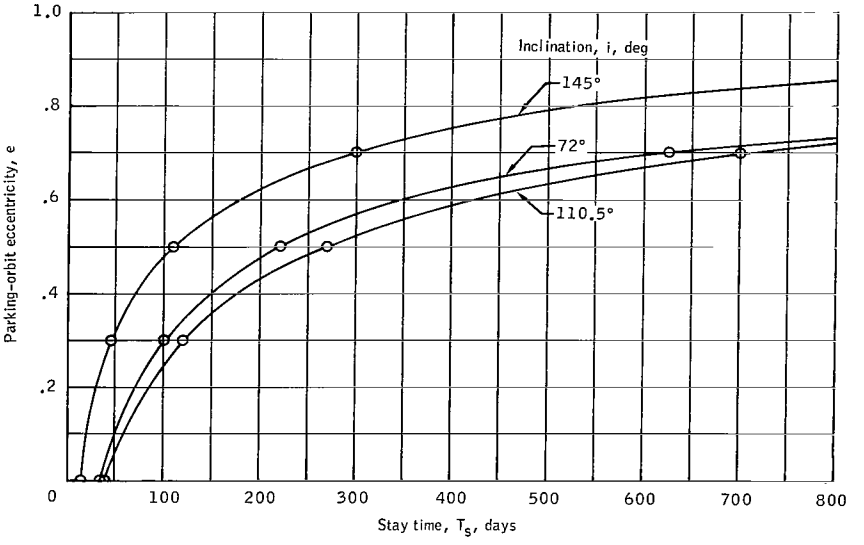

Figure 7. - Variation of orbital eccentricity with stay time for a stationary V_∞ geometry.

V_∞ geometry. Three orbits were found to accommodate this geometry. As the stay time is shortened, accelerated rotation rates are required to insure final alinement with the departure asymptote, and progressively smaller orbital eccentricities are required to obtain the faster rates. Figure 8 indicates that a 145° inclined circular orbit would rotate through the required angles during a stay time as low as 20 days. The curves of figure 8 also show that orbits which are more highly inclined have correspondingly lower eccentricities.

Figures 8 and 9 show the characteristics of the highest energy regressing parking orbit which shifts into proper alinement for departure during the example mission. This is the parking orbit for which the MOI ΔV and TEI ΔV are given in figure 5, and corresponds to orbit 1 of table I. The dashed lines of figure 8 are the inertial traces of the orbital groundtrack for the first revolution after MOI and the final revolution prior to TEI 300 days later. This is the configuration of the parking orbit as it exists at the beginning of the mission window. The solid bell-shaped curve shows the position of periapsis at the time of MOI and TEI and at 50-day intervals during the orbital stay time. Also, the apparent path of the Sun around Mars is shown at 50-day intervals between MOI and TEI. Figure 8 illustrates several interesting characteristics of this parking orbit.

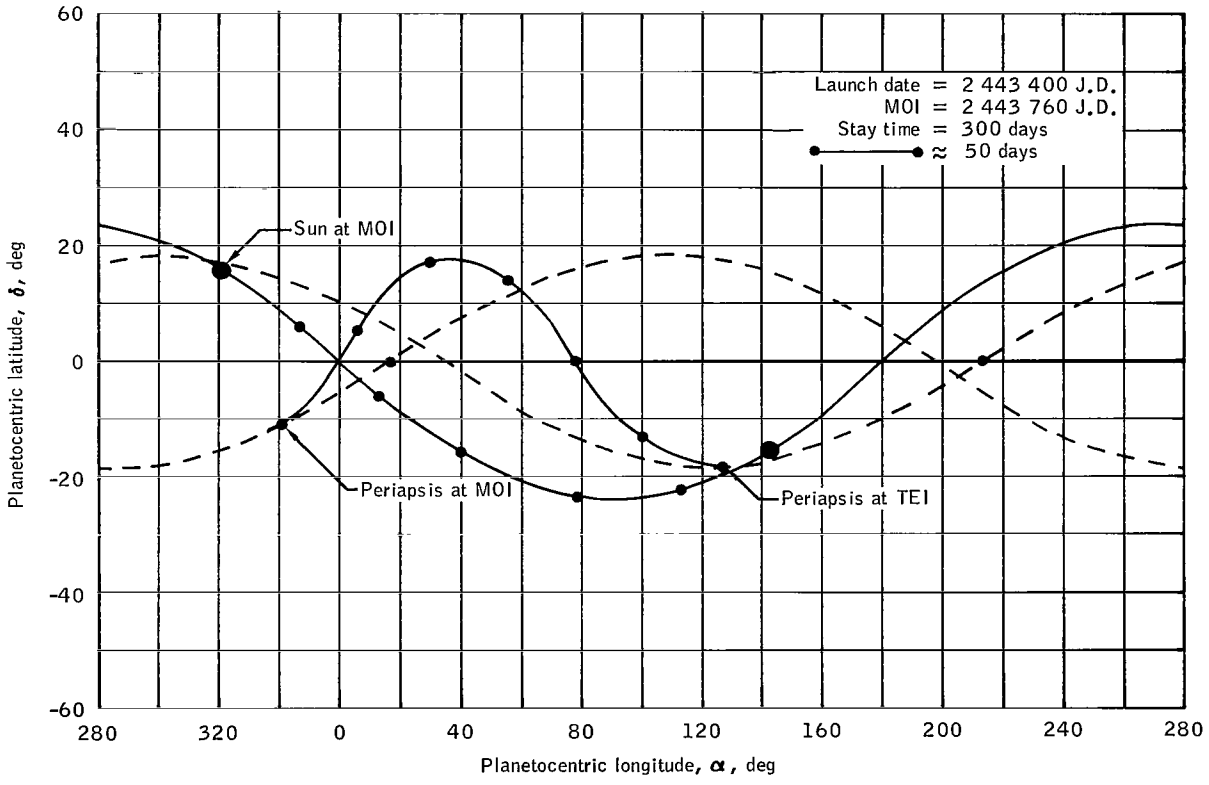

Figure 8. - Planetocentric motion of periapsis and the subsolar point for a typical high-energy parking orbit.

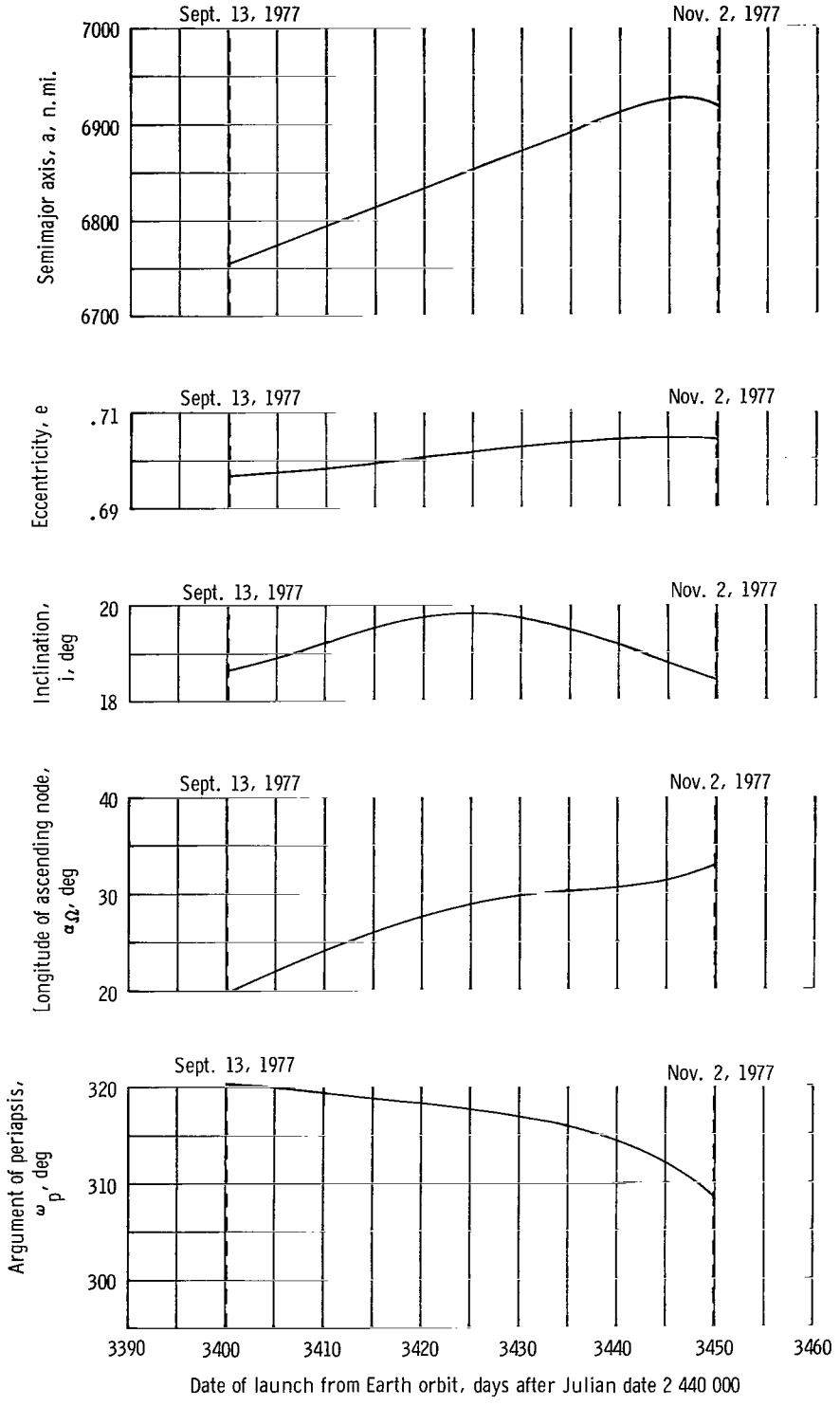

Figure 9. - Required characteristics of a regressing parking orbit and their variation during the 1977 mission window.

1. The parking-orbit periapsis sweeps through a wide range in latitude, from -12° to $+18.6^\circ$ and then back to -18.6°.

2. The periapsis crosses the Mars equator twice — about 40 days after MOI and again at 200 days after MOI. This fact would be crucial to minimize plane change requirements, should an equatorial parking orbit be desired, since the plane change could then be performed at the parking-orbit apoapsis.

3. The periapsis "chases" the Sun. Thus, periapsis will remain in sunlight for the entire planetary visit.

Figure 9 shows how the required characteristics of this high-energy orbit vary across the Earth-orbital launch window. Basically, the changing characteristics of this parking orbit reflect changes in the basic V_∞ geometry.

CONCLUDING REMARKS

Assuming the hyperbolic excess velocities and the periapsis altitude to be nonvarying, the eccentricity of the parking orbit is the fundamental quantity which governs the expense of the Mars-orbital insertion and transearth-injection impulsive velocities. The impulsive velocities are greatest for a circular parking orbit and diminish as the orbital eccentricity increases. From an impulsive-velocity standpoint, it is therefore advantageous to have the parking-orbit eccentricity as large as possible.

However, orbital eccentricity also governs the speed of rotation of the orbital node and periapsis position vectors. Circular orbits experience the fastest regression rates. For an orbital mission in which a large plane change must be realized during a short stay time, it may be necessary to adopt a near-circular parking orbit. In that case, less impulsive velocity may be required to insert into a high-eccentricity ellipse and make a parking-orbit plane change.

The important conclusions regarding the use of this technique therefore rest with the trade-off on orbital eccentricity. Obviously, any technique which requires a smaller eccentricity will have greater fuel costs. For long planetary stay times (300 to 500 days), this technique appears to be feasible for orbital eccentricities as large as 0.7 with periapsis altitudes of 200 n. mi. These orbits have inclinations on the order of 20°. Higher orbital eccentricities can be obtained by reducing the periapsis altitude or the orbital inclination.

Manned Spacecraft Center
National Aeronautics and Space Administration
Houston, Texas, April 16, 1968
981-30-10-00-72

REFERENCES

1. Luidens, Roger W.; and Miller, Brent A.: Efficient Planetary Parking Orbits With Examples for Mars. NASA TN D-3220, 1966.

2. Bird, John D.; Thomas, David F.; and Collins, Robert L.: An Investigation of a Manned Mission to Mars. Trajectories and Mission Analysis. Paper presented at the Manned Planetary Mission Technology Conference, Lewis Research Center, Cleveland Ohio, May 21-23, 1963. NASA TM X-50122, 1963.

3. Bird, John D.; and Thomas, David F.: Orbital Rendezvous Considerations for a Mars Mission. Advances in the Astronautical Sciences, vol. 16, part 1, p. 219. (Paper presented at AAS Symposium: Space Rendezvous, Rescue, and Recovery, Sept. 12, 1963.)

4. Lorell, J.: Long Term Behavior of Artificial Satellite Orbits Due to Third-Body Perturbations. J. Astron. Sci., Vol. XII, no. 4, Winter 1965, pp. 142-152.

5. Breakwell, J. V.; and Hensley, R. D.: An Investigation of High Eccentricity Orbits About Mars. First Compilation of Papers on Trajectory Analysis and Guidance Theory, NASA SP-141, 1967, pp. 175-215.

6. Gedeon, G. S.; Douglas, B. C.; and Palmiter, M. T.: Resonance Effects on Eccentric Satellite Orbits. J. Astron. Sci., Vol. XIV, no. 4, July-Aug. 1967, pp. 147-157.

7. Escobal, P. R.: Methods of Orbit Determination. John Wiley & Sons, Inc., 1965.

8. Anon.: Explanatory Supplement to the Astronomical Ephemeris and the American Ephemeris and Nautical Almanac. Her Majesty's Stationery Office (London), 1961.

9. Danby, J. M. A.: Fundamentals of Celestial Mechanics. The Macmillan Co., 1962.

TABLE I. - SUMMARY OF REGRESSING PARKING ORBITS WHICH SHIFT INTO ALINEMENT FOR DEPARTURE FOR THREE EARTH-ORBITAL LAUNCH DATES

(a) September 13, 1977

Orbit geometry	Orbit number	Inclination, deg	Eccentricity (a)	MOI ΔV, fps	TEI ΔV, fps	MOI ΔV + TEI ΔV, fps	Total mission ΔV, fps
1	1	18.64	0.6974	3397	3991	7 388	20 041
	2	68.28	.5611	3987	4581	8 568	21 222
	3	113.36	.4740	4379	4972	9 351	22 005
	4	140.92	.6114	3768	4361	8 129	20 783
2	5	72.18	0.3257	5071	5667	10 738	23 391
3	6	70.14	0.5557	4011	4607	8 618	21 272
	7	112.10	.4715	4391	4985	9 379	22 029
	8	141.10	.6360	3661	4255	7 916	20 570
4	9	70.95	0.3324	5039	5633	10 672	23 326
	10	95.04	.5105	4213	4807	9 020	21 674

[a]Periapsis altitude = 200 n. mi.

TABLE I. - SUMMARY OF REGRESSING PARKING ORBITS WHICH SHIFT INTO ALINEMENT FOR DEPARTURE FOR THREE EARTH-ORBITAL LAUNCH DATES - Continued

(b) October 9, 1977

Orbit geometry	Orbit number	Inclination, deg	Eccentricity (a)	MOI ΔV, fps	TEI ΔV, fps	MOI ΔV + TEI ΔV, fps	Total mission ΔV, fps
1	1	19.79	0.7018	3209	3788	6 997	18 823
	2	68.11	.5503	3865	4443	8 308	20 134
	3	113.30	.4744	4207	4785	8 992	20 818
	4	141.55	.6125	3592	4170	7 762	19 588
2	5	59.56	0.4518	4311	4891	9 202	21 027
3	6	70.13	0.5446	3891	4469	8 360	20 186
	7	111.86	.4713	4221	4799	9 020	20 846
	8	141.88	.6417	3466	4044	7 510	19 336
4	9	58.29	0.4480	4329	4906	9 235	21 061
	10	70.94	.3242	4909	5487	10 396	22 222

[a]Periapsis altitude = 200 n. mi.

TABLE I. - SUMMARY OF REGRESSING PARKING ORBITS WHICH SHIFT INTO ALINEMENT FOR DEPARTURE FOR THREE EARTH-ORBITAL LAUNCH DATES - Concluded

(c) November 2, 1977

Orbit geometry	Orbit number	Inclination, deg	Eccentricity (a)	MOI ΔV, fps	TEI ΔV, fps	MOI ΔV + TEI ΔV, fps	Total mission ΔV, fps
1	1	18.46	0.7045	3429	3646	7 075	19 690
	2	67.84	.5513	4093	4311	8 404	21 018
	3	113.57	.4691	4463	4681	9 144	21 758
	4	141.39	.6041	3861	4079	7 940	20 554
2	5	71.82	0.3245	5139	5357	10 496	23 110
3	6	69.89	0.5501	4101	4317	8 418	21 032
	7	111.86	.4655	4479	4697	9 176	21 790
	8	141.72	.6384	3712	3930	7 642	20 256
4	9	58.44	0.4505	4550	4765	9 315	21 929
	10	71.24	.3278	5126	5340	10 466	23 080

[a]Periapsis altitude = 200 n. mi.

TABLE II. - ORBITAL GEOMETRY CODE

Orbital geometry of regression	Orbital configuration relative to the approach asymptote	Orbital configuration relative to the departure asymptote
1	$\Omega_{1,A}$	$\Omega_{1,D}$
2	$\Omega_{1,A}$	$\Omega_{2,D}$
3	$\Omega_{2,A}$	$\Omega_{1,D}$
4	$\Omega_{2,A}$	$\Omega_{2,D}$

NASA-Langley, 1968 —— 30 S-169

"The aeronautical and space activities of the United States shall be conducted so as to contribute . . . to the expansion of human knowledge of phenomena in the atmosphere and space. The Administration shall provide for the widest practicable and appropriate dissemination of information concerning its activities and the results thereof."

—NATIONAL AERONAUTICS AND SPACE ACT OF 1958

NASA SCIENTIFIC AND TECHNICAL PUBLICATIONS

TECHNICAL REPORTS: Scientific and technical information considered important, complete, and a lasting contribution to existing knowledge.

TECHNICAL NOTES: Information less broad in scope but nevertheless of importance as a contribution to existing knowledge.

TECHNICAL MEMORANDUMS: Information receiving limited distribution because of preliminary data, security classification, or other reasons.

CONTRACTOR REPORTS: Scientific and technical information generated under a NASA contract or grant and considered an important contribution to existing knowledge.

TECHNICAL TRANSLATIONS: Information published in a foreign language considered to merit NASA distribution in English.

SPECIAL PUBLICATIONS: Information derived from or of value to NASA activities. Publications include conference proceedings, monographs, data compilations, handbooks, sourcebooks, and special bibliographies.

TECHNOLOGY UTILIZATION PUBLICATIONS: Information on technology used by NASA that may be of particular interest in commercial and other non-aerospace applications. Publications include Tech Briefs, Technology Utilization Reports and Notes, and Technology Surveys.

Details on the availability of these publications may be obtained from:

SCIENTIFIC AND TECHNICAL INFORMATION DIVISION

NATIONAL AERONAUTICS AND SPACE ADMINISTRATION

Washington, D.C. 20546